

Changing accretion geometry of Seyfert 1 Mrk 335 with *NuSTAR*: A comparative study

Santanu Mondal*  and C. S. Stalin

¹ Indian Institute of Astrophysics, II Block, Koramangala, Bangaluru, 560034, India; santanu.mondal@iiap.res.in

* Correspondence: santanu.mondal@iiap.res.in

Abstract: We present a detailed spectral study of the narrow-line Seyfert 1 galaxy, Markarian 335, using eight epochs observations made between 2013 and 2020 with the *Nuclear Spectroscopic Telescope Array*. The source was variable during this period both in spectral flux and flow geometry. We estimated the height of the Compton cloud from the model fitted parameters for the whole observation period. This allowed us to investigate the underlying physical processes that drive the variability in X-rays. Our model fitted mass varies in a narrow range, between $(2.44 \pm 0.45 - 3.04 \pm 0.56) \times 10^7 M_{\odot}$, however, given the large error bars, is consistent with being constant and is in agreement with that known from optical reverberation mapping observations. The disk mass accretion rate reached maximum, 10% of the Eddington rate during June 2013. Our study puts light on mass outflows from the system and also compares different aspects of accretion with X-ray binaries.

Keywords: galaxies: active; galaxies: jets; galaxies: nuclei; radiative transfer; Seyfert 1 objects: individual: Mrk 335

1. Introduction

Active galactic nuclei (AGN) host an accretion disk with an energetic X-ray producing Compton cloud so-called corona around a supermassive black hole at the center. The emitted X-ray radiation also acts as one of the most direct probes of accretion onto AGN. They show rapid flux and polarization variations which indicate that the observed high energy radiation mainly originates from the inner few to tens of Schwarzschild radii ($r_s = 2GM_{\text{BH}}/c^2$, M_{BH} , G, and c are the mass of the black hole, gravitational constant and the speed of light respectively) from the event horizon of the black hole [1]. The power-law (PL) component is widely accepted as the effect of inverse Compton (IC) scattering of thermally produced soft photons from the accretion disk by a corona of hot electrons at the inner edge of the disk [2,3]. However, the geometry and size of the corona as well as the physical mechanisms governing the energy transfer between the disk and the corona are not well understood, which necessitates a physical model to better understand the observed signatures in them.

There are proposed models in the literature [4] which consider the corona to be the region between the truncation radius and the innermost stable circular orbit. However, it is not clear why the disk truncates at a certain radius from the central black hole and how the truncation radius is connected with the corona. Furthermore, most of the models in the literature [5,6] use optical depth or the coronal temperature or the spectral index as a parameter to compute the spectrum from the corona. None of them are the basic physical quantities of accretion. According to two-component advective flow model, TCAF [7,8], at a certain distance from the BH where gravitational force balances with the centrifugal force, shock forms by the low angular momentum, hot, sub-Keplerian halo, and satisfying Rankine-Hugoniot conditions, which is the region of the truncation of the disk. Apart from that as the two forces balances each other accreting matter virtually stops and its velocity goes down, which also increases the optical depth of the corona region. As the gravitational force dominates closer to the BH, velocity again increases and the flow passes through the inner sonic point and falls onto



Citation: Mondal, S.; Stalin, C. S. Changing accretion geometry of Seyfert 1 Mrk 335 with *NuSTAR*: A comparative study. *Preprints* 2021, 9, 21. <https://doi.org/>

Received:

Accepted:

Published:

Publisher's Note: MDPI stays neutral with regard to jurisdictional claims in published maps and institutional affiliations.

the BH, therefore the flow is transonic [7]. Beyond this shocked region, both the disk and halo matter pile up to decide the optical depth and temperature of the corona region. The same region also upscatters the incoming soft radiation from the disk via IC. A typical X-ray spectrum of AGN in the 2-10 keV shows primarily the signature of PL. Due to IC, the corona cools down and its area decreases, leading to low brightness level and a softer spectrum [9]. These physical properties and the dynamics of the flow makes the TCAF more favourable as a physical model than other existing models in the literature. In addition to the above, TCAF uses mass accretion rates and the mass of the BH as model parameters, which are the basic physical quantities of a flow. Furthermore, the same shock location which can explain the spectral features, can also be able to explain the temporal features from its oscillation [10,11]. Therefore, among the various models available in the literature to understand the observed X-ray emission in AGN, we preferred to consider TCAF model for our study.

TCAF model has mainly five parameters: (i) mass of the black hole (M_{BH}), (ii) disk accretion rate (\dot{m}_d), (iii) halo accretion rate (\dot{m}_h), (iv) location of the shock (X_s), and (v) shock compression ratio (R). Increasing \dot{m}_d keeping the other parameters fixed, increases the number of soft photons from the Keplerian disk [12] making the spectrum softer. Higher \dot{m}_h increases the corona temperature and hardens the spectrum. Similarly increase of either X_s or R lead to hardening of the spectrum. However, in reality all parameters change in multidimensional space. Therefore such variations may not sustain due to non-linear change in optical depth and coronal temperature in different epochs. A detailed parameter study has been made in Ref. [13]. In recent years, TCAF model is implemented in XSPEC and has been used widely to study both X-ray binaries (XRBs) [14–16] and AGN [17–19]. However, there are physical processes which are not yet incorporated in the current TCAF model e.g. jet, bulk motion Comptonization and the spin effect of the BH.

Apart from the above components, many AGN exhibit extra features in their X-ray spectra that likely originate from the accretion disk [20]. The so-called X-ray reflection features produced by the accretion disk might be because of its illumination from the central compact object, such as a magnetically dominated corona residing above the surface of the disk [e.g. 2,21,22]. A prominent feature in the X-ray spectrum is the Fe $K\alpha$ emission line at around 6.4 keV which is due to fluorescence in a dense and relatively cold medium [23–25]. The shape of the Fe $K\alpha$ line is a powerful probe of the general relativistic effects close to the BH [26,27], leading to estimates of the spin of the BH [28–30]. Indeed, observations over the last decades by X-ray satellites have uncovered relativistically broadened Fe $K\alpha$ line in the spectra of several AGN [31–33] and black hole XRBs [e.g. 34]. Models of X-ray reflection spectra [5,35] show additional features that collectively can constrain the ionization state, heating, and cooling of the illuminated surface [36].

Mrk 335 is a bright narrow-line Seyfert 1 (NLS1) galaxy at a redshift $z = 0.026$ [37], with a black hole mass, $M_{\text{BH}} = 2.6 \times 10^7 M_{\odot}$ [38] and showing ionized absorption in the X-ray and ultra-violet (UV) bands [39]. It has been observed to go into extremely low-flux states [40] where the soft X-ray flux dropped by a factor of up to ~ 30 , while the hard flux dropped only by a factor of ~ 2 in 7 years. Using observations from XMM-Newton, Ref. [41] found signatures of absorption and high reflection fraction in the spectrum of Mrk 335 in its lowest flux state, whereas at the intermediate flux state the observed X-ray spectra is explained well by blurred reflection model without the requirement of variable absorption [42]. Ref. [43] estimated a high-frequency lag of ~ 150 s between the continuum dominated energy bands and the iron line and soft excess components for this source. This time lag suggests that the continuum source is located very close to the central black hole and that relativistic effects are supposed to be worth considering. Using combined *Swift* and *NuSTAR* observations, Ref. [44] interpreted the X-ray flare during 2014 as arising from the vertical collimation and ejection of the X-ray emitting corona at a mildly relativistic velocity, that causes the continuum emission

Table 1: Log of observations.

Date	MJD	OBSID	Exposure (s)
2013-06-13	56456	60001041002	21299
2013-06-13	56456	60001041003	21525
2013-06-25	56468	60001041005	93028
2014-09-20	56920	80001020002	68908
2018-07-10	58309	80201001002	82257
2020-06-06	59006	90602619004	30156
2020-06-07	59007	90602619006	30495
2020-06-08	59008	90602619008	22452

to be relativistically beamed away from the disk. Ref. [45] discussed the effect of the geometry of the corona on the relativistically blurred X-ray reflection arising from the accretion disk, which can also explain the variability in between low and high-flux states. Ref. [46] performed the structure function analysis using long term *Swift* optical/UV and X-ray data of Mrk 335 and showed that the X-ray low flux state could be due to the physical changes in the corona or absorption, whereas the variability in the optical/UV band is more consistent with the thermal and dynamic timescales associated with the accretion disk. Ref. [47], studied the low-flux state data using *XMM-Newton* and observed absorption lines from a highly ionized outflowing wind.

Several studies on Mrk 335 clearly show that the system is highly variable leaving a range of possibilities in its dynamical behavior and emission features. Mrk 335 is known to show change in geometry [45], such a change in geometry can be found from a disk-based model fit such as TCAF to data. It is not clear to date if there is any change in the mass accretion of the source, and if so, what effects it can have on the geometry of the corona in the source? To investigate the above, in this work we chose this object and carried out an analysis of the X-ray data on the source acquired by *NuSTAR* during the period 2013-2020. This paper is organized as follows: in the next section, we describe the observation details and the analysis procedures. In §3, we explain our results obtained from model fits to the data and summarize our conclusions in the final section.

2. Observation and Data analysis

In the present manuscript, we analyzed archival data¹ of *NuSTAR* observations of Mrk 335 made during 2013-2020. During this time interval Mrk 335 was observed nine times, out of which in one observation, data quality is not good, so we considered the remaining eight observations. The details of the observations are listed in Table 1. The *NuSTAR* data in the energy range of 3.0–30 keV (as the data is noisy above 30 keV), were extracted using the standard NUSTARDAS v1.3.1² software. We ran NUPIPELINE task to produce cleaned event lists and NUPRODUCTS for generation of the spectra. We used a region of 80'' for the source and 100'' for the background using ds9. The data were grouped by *grppha* command, with a minimum of 30 counts per energy bin. The same binning was used for all the observations. For spectral analysis of the data we used XSPEC³ [49] version 12.8.1. We used the absorption model TBABS [48] with the Galactic hydrogen column density fixed at 3.6×10^{20} atoms cm^{-2} [50] throughout the analysis.

¹ <https://heasarc.gsfc.nasa.gov/docs/cgro/db-perl/W3Browse/w3browse.pl>

² <https://heasarc.gsfc.nasa.gov/docs/nustar/analysis/>

³ <https://heasarc.gsfc.nasa.gov/xanadu/xspec/>

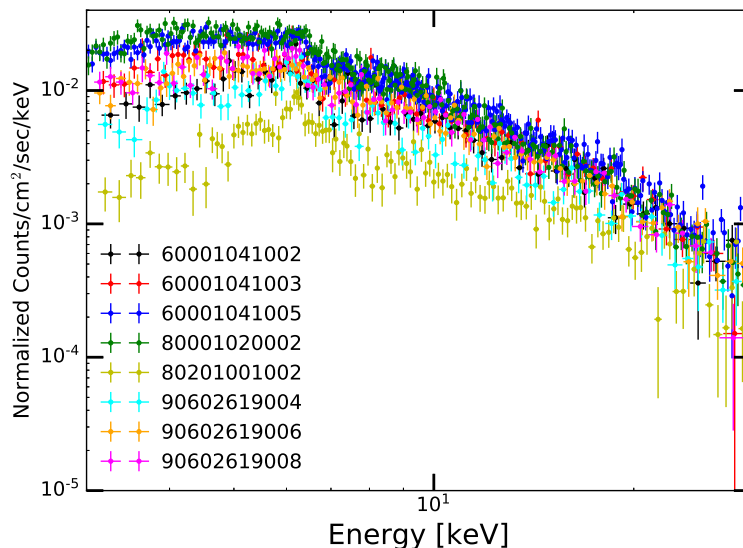


Figure 1. Spectra of all the eight observations in the 3–30 keV energy range. Variability of the source is evident.

3. Results and Discussion

We fit the *NuSTAR* observations of Mrk 335 taken between 2013 to 2020. During this observation period the source showed significant variability in spectral flux (see Figure 1). We did spectral analysis using different models. First, we performed spectral fitting using a simple powerlaw (PL) model as `TBABS(GAUSS+PL)`, where the PL index (Γ) varies from 0.72-1.84, a change by a factor greater than two, which is clearly an indication of significant change in the flow behavior and corona properties. The model fitted parameters are provided in Table 2. Our model fits show that the line energy and width vary in a broad range, which point to complex geometry changes and gravity effects (more especially line broadening) in the source. In addition to the simple PL model, we also modeled the observed spectra using the complex phenomenological model `PEXRAV` [51] and the physical model `TCAF` [8]. The results of `PEXRAV` model fits are given in Table 3. Our PL model fits indicate that the source passed through hard and soft spectral states similar to XRBs, where the timescale for changing from one state to other is in the order of few days to weeks, which is the viscous timescale [52, and references therein]. We found a similar timescale when the corona changed from its maximum size to minimum, which is around 12 days. However, as the viscous timescale for AGN is in the order of few hundred to few Myr (scaled by the mass of the BH), it may not be possible to observe the similar timescale for other AGNs. In future we aim to explore this aspect of accretion to estimate the viscosity of the flow.

From `PEXRAV` model fits, we found the reflection fraction to be high with $R_{\text{ref}} > 0.9$ for all the epochs. When the Fe abundance (A_{Fe}) was made as a free parameter, A_{Fe} was found to vary from sub-Solar to super Solar values during the epochs analysed here, which is quite unphysical. It has been pointed out by Ref. [53], reflection model fits to observed X-ray spectra are generally found to yield high A_{Fe} values. Also, according to Ref. [54], the high A_{Fe} obtained from model fits to data could be due to some unknown physical effects being overlooked in current models. Therefore, for `PEXRAV` model fits, we froze A_{Fe} to solar value. For the observation day MJD=56468, we required one extra Gaussian line component at low energy ~ 5 keV. From the line component and its width it can be seen, that both narrow and broad lines are present in this epoch. We kept the disk inclination (i_{inc}) fixed to 45° throughout

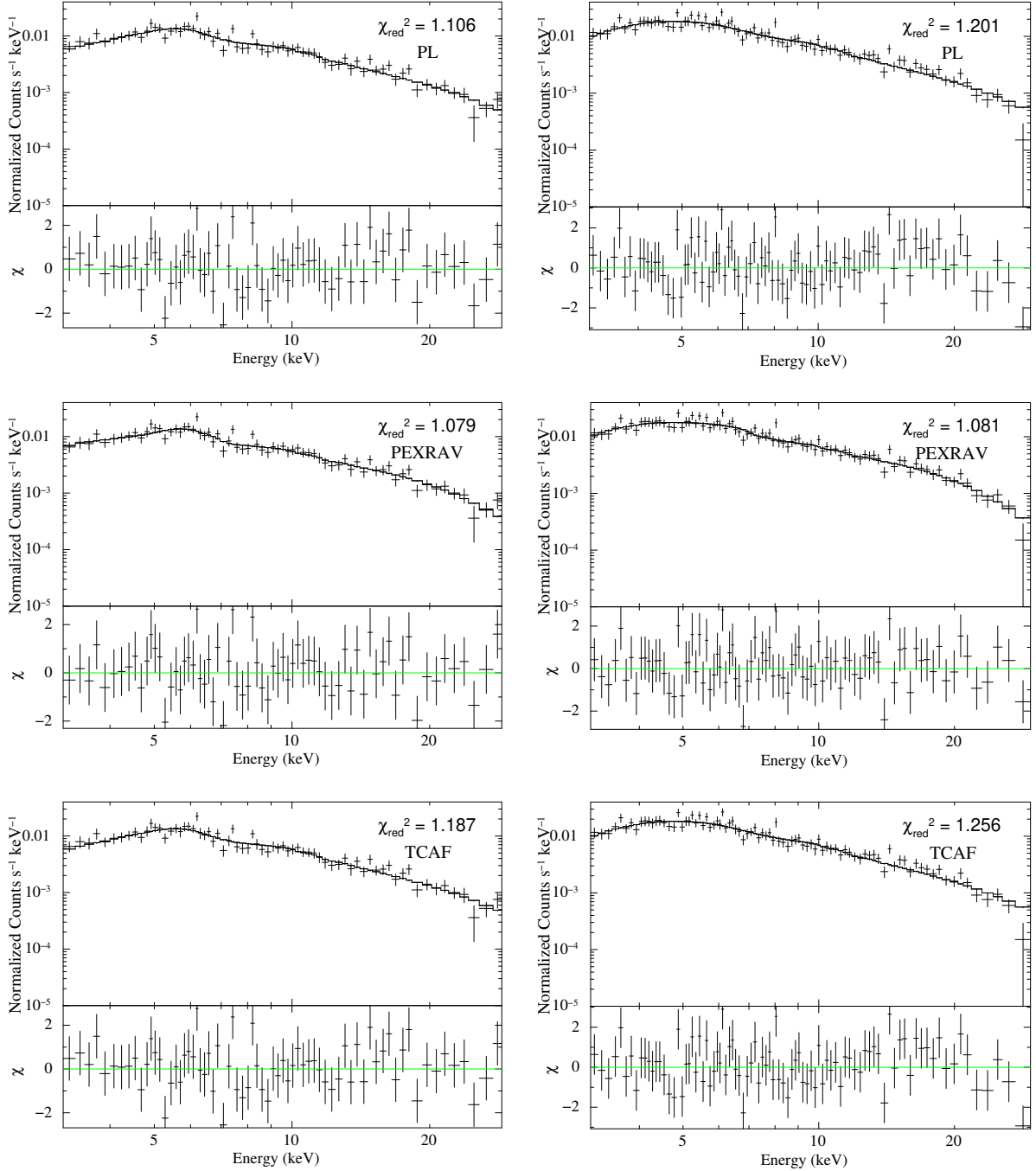


Figure 2. Sample fit of 3–30 keV spectra with PL, PEXRAV, and TCAF models for OBSIDs 60001041002 (left panel) and 60001041003 (right panel) along with the residuals.

[55]. Next we applied the physical model TCAF and having the form TBABS(TCAF+GAUSS) to extract the accretion flow parameters. For all observations goodness of the fit is more or less similar to PEXRAV model. The TCAF model fitted parameters are provided in Table 4. For some observations, better fits were achieved after adding some additive model components which are detailed in the table. For majority of the epochs, the χ^2/dof obtained from PEXRAV and TCAF model fits are in agreement, which for three epochs, the χ^2/dof from TCAF fits are marginally larger than those obtained from PEXRAV model fits. This might be due to differences in the spectral components between models e.g. TCAF does not include line features, that may give relatively higher χ^2/dof . In Figure 2, we show different model fitted spectra for the OBSID 60001041002/3 in the left/right panels of the figure. Figure 3 shows the same spectral fitting but for the OBSID 60001041005 (left panel) and 80001020002 (right panel). The rest of the observational fits are shown in Appendix.

We used TCAF model fitted parameters to estimate the geometrical height of the shock (H_{shk}). The height of the corona is basically the height of the shock, as the shock is the boundary layer of the corona. We estimated (H_{shk}) using the equation below [see also 14]:

$$H_{shk} = \left[\frac{\gamma(R-1)X_s^2}{R^2} \right]^{1/2}, \quad (1)$$

where, γ is the adiabatic index, X_s is the location of the shock or the boundary of the corona, and R is the shock compression ratio ($= \rho_+ / \rho_-$), a ratio of the density of the downstream to the density of the upstream of the flow.

In Figure 4, we show the variation of various model parameters obtained from TCAF model fits as well as the variation of hardness ratio (HR) with time. The halo rate was always higher than the disk rate by an order of magnitude or more which implies that the flow was dominated by the low angular momentum matter, which might be accreted from the wind or host galaxies. The \dot{m}_d was found to vary by a factor of ~ 40 from 0.24% to 10% of the Eddington rate and the \dot{m}_h varied between 1.2-3.1 Eddington rate. The size of the shock location (X_s) or corona changed significantly and reached up to $6 r_s$ during 25 June 2013 (60001041005) and $8 r_s$ during 2014 (80001020002). For the OBSID 60001041005, we required an extra broad (1.55 keV) Gaussian component at low energy 3.44 keV, which was also found to be broadened by strong gravitational effects [27]. For the OBSID 80001020002, we required an additive DISKLINE [26] component at line energy 6.12 keV with emissivity powerlaw index (β) ~ -3.0 and $R_{in} = 24.4 r_g (GM/c^2)$ as the current TCAF model does not include line emission due to gravitational effect in the fit. It is worth noting that the X_s is achieved for the highest \dot{m}_d , which might be due to the cooling effect inside the corona. As the accretion rate increased more disk photons got intercepted by the corona. This cooled the corona, causing the shock to move inwards and thus causing a significant change in the size of the corona. Such change in the corona could also be due to the activity of the jet, which extracted a significant amount of thermal energy and contracted the corona [58]. Therefore it is also possible to establish a jet-disk connection using TCAF model fits to AGN spectra similar to XRBs [59–61, and references therein].

Such movement of the shock can give rise to the observed variability in spectral and temporal properties [62]. During 2014, \dot{m}_h further increased and made the corona hotter and shock the receded slightly. During 2018, shock further moved away, the corona has become bigger in size, therefore intercepts more soft photons, generates high energy photons, which can also ionize the disk atmosphere. For this particular observation, we required partial covering fraction model (ZXIPCF), with a covering factor ($f_c=0.45$) and low ionization parameter ($\log \xi=1.2$). For the OBSID 90602619004, during 2020, we required another narrow line (0.29 keV) component, when the shock again moved inward. The model fitted shock compression ratio also varied in a broad range, which also dictates the strength of the shock

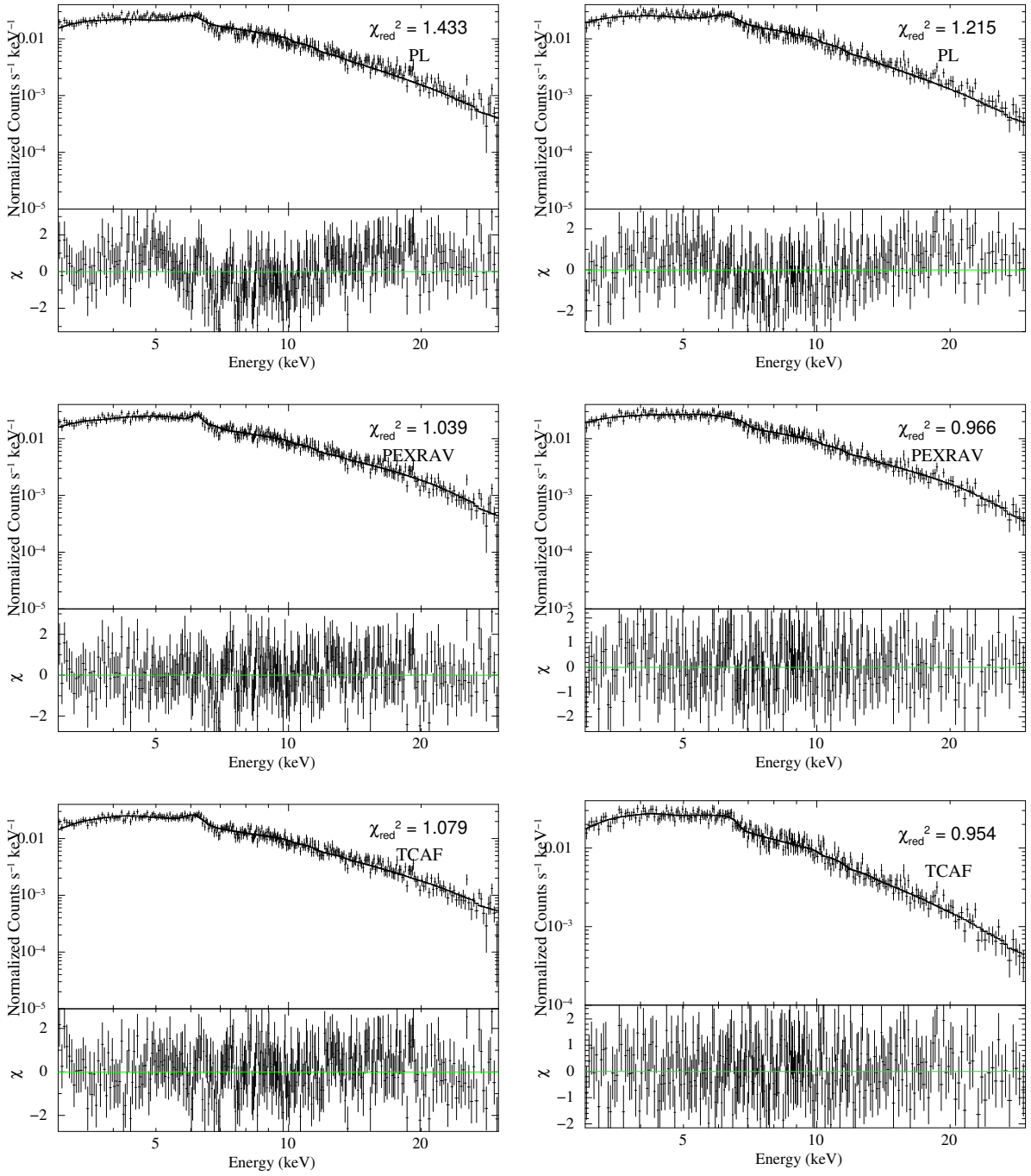


Figure 3. Same as Figure 2 but for the OBSIDs 60001041005 (left panel) and 80001020002 (right panel) along with the residuals.

Table 2: Best-fitting parameters with the TBABS(GAUSS+PL) model.

OBSID	Γ_{PL}	$N_{\text{PL}} (\times 10^{-4})$ <i>ph./keV/cm²/s</i>	E_g [keV]	σ_g [keV]	χ^2/dof
60001041002	1.09 ± 0.08	2.15 ± 0.46	5.47 ± 0.18	0.79 ± 0.21	71.91/65
60001041003	1.12 ± 0.10	2.79 ± 0.76	4.21 ± 0.45	1.52 ± 0.34	102.1/85
60001041005	1.66 ± 0.02	13.58 ± 0.54	6.00 ± 0.99	0.28 ± 0.06	452.94/316
80001020002	1.84 ± 0.02	20.92 ± 0.91	6.20 ± 0.13	0.34 ± 0.08	320.71/264
80201001002	0.72 ± 0.06	0.40 ± 0.06	6.07 ± 0.07	0.60 ± 0.08	136.14/124
90602619004	1.24 ± 0.06	2.50 ± 0.33	6.08 ± 0.07	0.41 ± 0.08	107.16/79
90602619006	1.17 ± 0.09	2.93 ± 0.71	4.83 ± 0.31	1.26 ± 0.30	82.39/106
90602619008	1.46 ± 0.05	6.07 ± 0.61	6.10 ± 0.06	0.13 ± 0.09	92.29/80

Γ_{PL} and N_{PL} are the PL index and normalization. E_g and σ_g are the Gaussian line energy and width respectively.

Table 3: Best-fitting parameters with the TBABS(PEXRAV+GAUSS) model.

OBSID	Γ	E_{cut} [keV]	R_{ref}	E_g [keV]	σ_g [keV]	χ^2/dof
60001041002	1.44 ± 0.03	31.55 ± 6.51	3.40 ± 1.17	5.66 ± 0.09	0.61 ± 0.21	68.01/63
60001041003	1.12 ± 0.02	16.56 ± 2.42	4.85 ± 1.07	3.40 ± 0.17	1.99 ± 0.37	89.72/83
60001041005 ^a	1.95 ± 0.10	96.30 ± 20.87	2.40 ± 0.41	6.20 ± 0.06	0.007 ± 0.003	323.19/311
80001020002	2.11 ± 0.09	107.90 ± 30.15	2.33 ± 0.92	5.50 ± 0.17	0.84 ± 0.17	253.39/262
80201001002	0.87 ± 0.03	20.40 ± 3.93	3.68 ± 0.81	6.09 ± 0.08	0.62 ± 0.08	128.70/122
90602619004	1.68 ± 0.03	54.63 ± 11.71	3.47 ± 1.12	6.11 ± 0.08	0.39 ± 0.09	96.97/77
90602619006	1.39 ± 0.02	69.19 ± 15.89	0.92 ± 0.17	5.20 ± 0.28	1.01 ± 0.36	81.39/104
90602619008	1.99 ± 0.04	32.69 ± 4.01	7.67 ± 1.07	6.12 ± 0.06	0.013 ± 0.003	78.82/78

Γ , E_{cut} , and R_{ref} are model PL photon index, cutoff energy, and reflection scaling factor respectively. E_g and σ_g are the Gaussian line energy and width. We kept the disk inclination fixed at 45° [55] and A_{Fe} at Solar abundance value. a: Gaussian component was added at 5.02 ± 0.18 keV with line width 0.64 ± 0.20 keV. The origin of this line is not clear yet, however, a similar line was observed for Mrk 335 earlier [56].

Table 4: Best-fitting parameters with the TBABS(TCAF+GAUSS).

OBSID	$M_{\text{BH}} \times 10^7$ [M_\odot]	\dot{m}_d [\dot{M}_{Edd}]	\dot{m}_h [\dot{M}_{Edd}]	X_s [r_s]	R	E_g [keV]	σ_g [keV]	χ^2/dof
60001041002	2.94 ± 0.63	0.0024 ± 0.0008	2.000 ± 0.725	22.43 ± 9.96	2.45 ± 0.54	5.58 ± 0.19	0.69 ± 0.21	72.45/61
60001041003	3.02 ± 0.60	0.0026 ± 0.0010	1.158 ± 0.331	43.72 ± 12.97	5.78 ± 1.23	4.18 ± 0.61	1.53 ± 0.52	101.75/81
60001041005 ^a	2.44 ± 0.45	0.1001 ± 0.0433	1.781 ± 0.143	6.24 ± 0.94	5.21 ± 1.26	6.10 ± 0.05	0.22 ± 0.07	333.54/309
80001020002 ^b	2.93 ± 0.65	0.0059 ± 0.0001	3.117 ± 0.181	8.66 ± 1.66	1.49 ± 0.17	2.13 ± 0.52	2.27 ± 0.95	244.18/256
80201001002 ^c	2.79 ± 0.70	0.0145 ± 0.0011	3.017 ± 0.144	33.53 ± 7.62	4.24 ± 1.39	6.02 ± 0.13	0.66 ± 0.15	130.29/117
90602619004 ^d	3.02 ± 0.98	0.0059 ± 0.0014	2.945 ± 0.365	21.25 ± 3.19	2.79 ± 0.62	6.01 ± 0.08	0.51 ± 0.09	87.65/72
90602619006	3.04 ± 0.56	0.0024 ± 0.0007	1.978 ± 0.150	21.54 ± 2.57	2.20 ± 0.26	4.78 ± 0.62	1.29 ± 0.49	82.35/102
90602619008	2.87 ± 0.95	0.0045 ± 0.0012	1.540 ± 0.259	22.22 ± 2.49	1.20 ± 0.13	5.53 ± 0.19	0.70 ± 0.22	95.42/76

\dot{m}_h , and \dot{m}_d represent TBABS(TCAF+GAUSS) model fitted sub-Keplerian (halo) and Keplerian (disk) rates respectively. X_s , and R are the model fitted shock location and shock compression ratio values respectively. E_g and σ_g are the Gaussian line energy and width. a: Gaussian component was added at 3.44 ± 0.07 keV with line width 1.55 ± 0.21 keV. b: DISKLINE [26] component was added with line energy at 6.12 ± 0.10 keV, powerlaw of emissivity (β)= -2.98 ± 0.70 , inner radius (R_{in})= $34.6 \pm 24.4 r_g (GM/c^2)$, and the disk inclination was frozen at 45° . c: ZXIPCF [57] multiplicative model component is used for parameters: column density (N_{H}) = $68 \pm 10.91 \times 10^{22} \text{cm}^{-2}$, covering fraction (f_c) = 0.45 ± 0.05 , $\log \xi = 1.2 \pm 0.3$. d: Gaussian component was added at 4.16 ± 0.11 keV with line width 0.29 ± 0.14 keV.

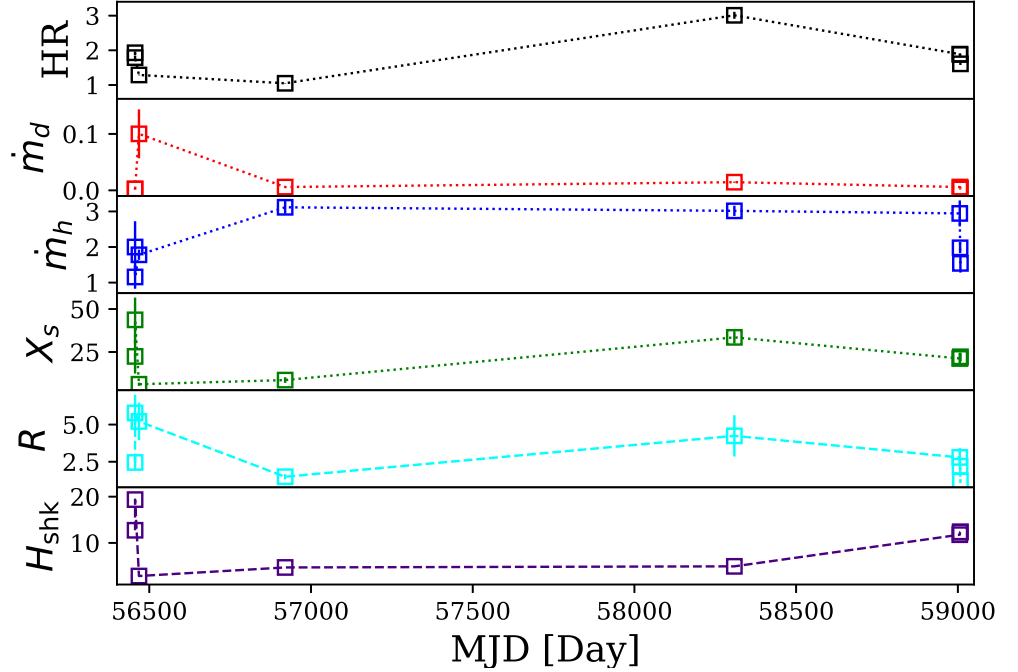


Figure 4. TCAF model fitted parameters evolution with observation days are shown along with HR estimated from the PL model fitted fluxes.

and the optical depth of the corona. The 5th panel of Figure 4 (from top) shows the variation of this parameter. The bottom panel of Figure 4, shows the estimated height of the corona, which changes significantly for the whole observation period.

Mass of the BH is one of the parameters in TCAF. Therefore, keeping it as a free parameter during TCAF model fits to the observed spectra will yield M_{BH} value for Mrk 335. We kept M_{BH} as a free parameter during our fitting and we found M_{BH} to vary in range between $(2.44 \pm 0.45 \text{ to } 3.04 \pm 0.56) \times 10^7 M_{\odot}$. Considering the large error bars the derived BH mass is consistent to be constant. Our derived M_{BH} is consistent with that estimated by [38] using optical reverberation mapping observations, however, an order of magnitude larger than that obtained by [53]. Such a low mass found by [53] could be due to them not considering an expanded corona in their model fit to the data. Our results on M_{BH} also shows that by fitting accretion disk based models such as TCAF to observed X-ray spectra one can estimate mass of BH in AGN. Also, we found that freezing M_{BH} to some fixed value from the above range and redoing the fit has negligible effect on other derived parameters, such as \dot{m}_d , \dot{m}_h , X_s , and R .

The viscous time scale in AGN is much longer compared to that of XRBs. At small time scales (in the order of few days or month) significant change in the accretion rate is not expected, similar is the case with the heating and cooling rates. Thus at such timescales, variability is expected to be less. This is in fact observed in the radio-quiet category of AGN and accretion disk based models can explain the observed flux variations in them. However, this might not be the case in the radio loud category of AGN, as relativistic jets play a dominant role in the flux variations observed in them. Even in those sources as the ejection of jets extract thermal energy from the corona, the change in the shock location can be drastic in them though the cooling is less. Results on this will be reported elsewhere.

4. Conclusion

In the present paper, we analyzed *NuSTAR* data of Mrk 335, observed between 2013-2020 to understand the dynamics of the flow and the accretion behavior of the source. We found that the source was significantly variable both in spectral flux, accretion geometry, and reflection fraction. We also found the geometry of the corona to change between epochs. Such a change can affect the reflection fraction and the spectral energy distribution of the illuminating radiation, and consequently the ionization rate. From the TCAF model fits we obtained the dynamics of the flow along with the geometry change of the corona and accretion rates. In our TCAF model fits, the line profiles due to relativistic effects were taken into account using an additive DISKLINE model where ever needed rather than using throughout for all observations. Among other models, even though the XILLVER model has relativistic and reflection effects incorporated, the accretion dynamics and the origin of corona are still lacking in the model. Therefore we did not take into account such models in our current study. Below we provide the key findings on the variable nature of the source:

1. During 2013, the corona at the inner region has changed significantly from its elongated stage ($\sim r_s$) to destruction stage $\sim 6r_s$, consistent with Ref. [44]. As the compression ratio has changed and the corona has contracted significantly, it can be possible that jet/mass outflow was launched around June 13, 2013, therefore a significant amount of thermal energy has been extracted by the jet/outflow and the corona contracted.
2. The observation during 2014, required a blurred reflection component along with TCAF to fit the spectra. This is quite natural as the corona contracted, the inner edge of the disk moved significantly inward, therefore the gravitational effect became dominant [26,27] and blurred the Fe K α line. We also required a broad Gaussian line component at ~ 2 keV.
3. The HR was roughly constant during 2013, and is also similar to that obtained during 2014.
4. There is a significant change in Γ_{PL} between 2013 and 2014 spectra, which can be due to sudden change in accretion rates. During this period disk accretion had increased by a factor of a few and also the size of the corona contracted significantly.
5. The steepening of the emissivity profile of Mrk 335 indicates that the corona is compact for this source [44]. In our study, we found that the size of the corona is indeed small and compact during 25th June 2013 and 20th September 2014 (see Table 4). It is also noticeable that the height of the corona reduced significantly during these two epochs.
6. During 2014, spectral flux between 3-30 keV changed/increased by a factor of ~ 3 compared to 2013 and 2018. This could be due to an increase in accretion rates as well as the change in corona. As the accretion rate increased (in 25th June 2013 and 10th July 2018), the number of soft photons increased, thereby increasing the cooling rate, i.e reduction of more energy from the corona by the seed photons from the Keplerian disk [see theoretical aspects in 9]. It should be noted that though the shock location changed significantly, the other parameters triggered that change, mainly the increase in disk accretion rate, therefore the cooling rate. This also infers that not only the shock location but other parameters are equally important to explain the observed variability.
7. During 2018 and onward, the corona and H_{shk} again elongated. During this period the HR also increased. This also implies that there is a correlation between HR and the geometry of the corona.
8. During 2018, to take into account the disk ionization effects along with TCAF, we required partial covering, ZXIPCF model to better fit the data. The model fit showed an absorption column density with $N_H = 6.8 \times 10^{23} \text{ cm}^{-2}$ is present. The fit also required a low ionization with, $\log \xi = 1.2 \text{ erg cm s}^{-1}$ with partial covering fraction of 0.45. This added component also indicates the presence of mass outflow from the system, which is

evident in the monitoring observations of the source in optical/UV and X-rays [63,64, and references therein].

9. The reflection fraction, R_{ref} , is measured as the ratio of the photon fluxes from the blurred reflection and powerlaw continuum model components. From PEXRAV model fitting we found this value > 0.9 .
10. The mass of the black hole which is kept as a free parameter is found to vary in a very narrow range $(2.44-3.04) \times 10^7 M_{\odot}$, and considering the error bars is consistent with a constant. This is in agreement with that of Ref. [38].
11. Earlier studies on observed X-ray variability inferred the origin of flux variations to changes in the primary powerlaw continuum possibly exhibited through intrinsic variations in the corona, or possible changes in its size or location [42,44,65]. This is in agreement with our present findings.

Author Contributions: “Conceptualization, methodology, formal analysis, writing—original draft preparation, Santanu Mondal; conceptualization, supervision, writing—review and editing, C. S. Stalin.”

Funding: Not Applicable

Institutional Review Board Statement: Not Applicable

Informed Consent Statement: Not Applicable

Data Availability Statement: We used archival data for our analysis in this manuscript. Appropriate links are given in the manuscript. For the details of the data fitting, one can directly contact to the first author.

Acknowledgments: We thank both referees for their constructive and insightful suggestions that improved the quality of the manuscript. SM acknowledges Ramanujan Fellowship (# RJF/2020/000113) by SERB, Govt. of India. This research has made use of the *NuSTAR* Data Analysis Software (NUSTARDAS) jointly developed by the ASI Science Data Center (ASDC), Italy and the California Institute of Technology (Caltech), USA. This research has also made use of data obtained through the High Energy Astrophysics Science Archive Research Center Online Service, provided by NASA/Goddard Space Flight Center.

Conflicts of Interest: “The authors declare no conflict of interest.”

References

1. McHardy I. M.; Koending E.; Knigge C.; Uttley P.; Fender R. P. Active galactic nuclei as scaled-up Galactic black holes. *Nature* 2006, 444, 730
2. Haardt F.; Maraschi L. A Two-Phase Model for the X-Ray Emission from Seyfert Galaxie. *ApJ* 1991, 380, L51
3. Zdziarski A. A.; Poutanen J.; Johnson W. N. Observations of Seyfert Galaxies by OSSE and Parameters of Their X-Ray/Gamma-Ray Sources. *ApJ* 2000, 542, 703
4. Esin A. A.; McClintock J. E.; Narayan R. Advection-Dominated Accretion and the Spectral States of Black Hole X-Ray Binaries: Application to Nova Muscae 1991. *ApJ* 1997, 489, 865
5. Garcia J.; Dauser T.; Reynolds C. S.; Kallman T. R.; McClintock J. E.; Wilms J.; Eikmann W. X-Ray Reflected Spectra from Accretion Disk Models. III. A Complete Grid of Ionized Reflection Calculations. *ApJ* 2013, 768, 146
6. Titarchuk L. Generalized Comptonization Models and Application to the Recent High-Energy Observations. *ApJ* 1994, 434, 570
7. Chakrabarti S. K. Standing Rankine-Hugoniot Shocks in the Hybrid Model Flows of the Black Hole Accretion and Winds. *ApJ* 1989, 347, 365
8. Chakrabarti S.; Titarchuk L. G. Spectral Properties of Accretion Disks around Galactic and Extragalactic Black Holes. *ApJ* 1995, 455, 623
9. Mondal S.; Chakrabarti S. K. Spectral properties of two-component advective flows with standing shocks in the presence of Comptonization. *MNRAS* 2013, 431, 2716
10. Chakrabarti S. K.; Mondal, S.; Debnath, D. Resonance condition and low-frequency quasi-periodic oscillations of the outbursting source H 1743- 322. *MNRAS* 2015, 452, 3451
11. Molteni D.; Sponholtz H.; Chakrabarti, S. K. Resonance oscillation of radiative shock waves in accretion disks around compact objects. *ApJ* 1996, 457, 805

12. Shakura N. I.; Sunyaev R. A. Black holes in binary systems. Observational appearance. *A&A* 1973, 24, 337
13. Chakrabarti S. K. Spectral properties of accretion disks around black holes. II. Sub-Keplerian flows with and without shocks. *ApJ* 1997, 484, 313
14. Debnath, D.; Chakrabarti, S. K.; Mondal, S. Implementation of two-component advective flow solution in xspec. *MNRAS* 2014, 440L, 121
15. Debnath, D.; Mondal, S.; Chakrabarti, S. K.; Characterization of GX 339-4 outburst of 2010-11: analysis by XSPEC using two component advective flow model. *MNRAS* 2015, 447, 1984
16. Mondal S.; Debnath D.; Chakrabarti S. K. Inference on Accretion Flow Dynamics Using TCAF Solution from the Analysis of Spectral Evolution of H 1743-322 during the 2010 Outburst. *ApJ* 2014, 786, 4
17. Mandal, S.; & Chakrabarti, S. K. Spectrum of Two-Component Flows around a Supermassive Black Hole: An Application to M87. *ApJ* 2008, 689, 17
18. Mondal, S.; Rani, P.; Stalin, C. S. *MNRAS* 2021, submitted
19. Nandi P.; Chakrabarti S. K.; Mondal S. Spectral Properties of NGC 4151 and the Estimation of Black Hole Mass Using TCAF Solution. *ApJ* 2019, 877, 65
20. Fabian A. C.; Ross R. R.; X-ray reflection. *SSRv* 2010, 157, 167
21. Galeev A. A.; Rosner R.; Vaiana G. S. Structured coronae of accretion disks. *ApJ* 1979, 229, 318
22. Merloni A.; & Fabian A. C. Thunderclouds and accretion discs: a model for the spectral and temporal variability of Seyfert 1 galaxies. *MNRAS* 2001, 328, 958
23. Barr P.; White N. E.; Page C. G. The discovery of low-level iron K line emission from CYG X-1. *MNRAS* 1985, 216, 65P
24. Nandra K.; Pounds K. A.; Stewart G. C.; Fabian A. C.; Rees M. J. Detection of iron features in the X-ray spectrum of the Seyfert I galaxy MCG -6-30-15. *MNRAS* 1989, 236, 39p
25. Pounds K. A.; Nandra K.; Stewart G. C.; George I. M.; Fabian A. C. X-ray reflection from cold matter in the nuclei of active galaxies. *Nature* 1990, 344, 132
26. Fabian A. C.; Rees M. J.; Stella L.; White N. E. X-ray fluorescence from the inner disc in Cygnus X-1. *MNRAS* 1989, 238, 729
27. Laor A. Line Profiles from a Disk around a Rotating Black Hole. *ApJ* 1991, 376, 90
28. Brenneman L. W.; Reynolds C. S. Constraining Black Hole Spin via X-Ray Spectroscopy. *ApJ* 2006, 652, 1028
29. Reynolds C. S. The spin of supermassive black holes. *Class. Quantum Gravity* 2013, 30, 244004
30. Reynolds C. S.; Fabian A. C. Broad Iron- K_{α} Emission Lines as a Diagnostic of Black Hole Spin. *ApJ* 2008, 675, 1048
31. Ballantyne D. R.; Vaughan S.; Fabian A. C. A two-component ionized reflection model of MCG-6-30-15. *MNRAS* 2003, 342, 239
32. Iwasawa K., et al. The variable iron K emission line in MCG-6-30-15. *MNRAS* 1996, 282, 1038
33. Risaliti G. et al. A rapidly spinning supermassive black hole at the centre of NGC 1365. *Nature* 2013, 494, 449
34. Mondal S.; Chakrabarti S. K.; Debnath D. Spectral study of GX 339-4 with TCAF using Swift and NuSTAR observation. *Ap&SS* 2016, 361, 309
35. Ross R. R.; Fabian A. C. A comprehensive range of X-ray ionized-reflection models. *MNRAS* 2005, 358, 211
36. Ross R. R.; Fabian A. C.; Young A. J. X-ray reflection spectra from ionized slabs. *MNRAS* 1999, 306, 461
37. Huchra J. P.; Vogeley M. S.; Geller M. J. The CFA Redshift Survey: Data for the South Galactic CAP. *ApJS* 1999, 121, 287
38. Grier C. J. et al. A Reverberation Lag for the High-ionization Component of the Broad-line Region in the Narrow-line Seyfert 1 Mrk 335. *ApJ* 2012, 744, L4
39. Longinotti A. L. et al. The Rise of an Ionized Wind in the Narrow-line Seyfert 1 Galaxy Mrk 335 Observed by XMM-Newton and HST. *ApJ* 2013, 766, 104
40. Grupe D.; Komossa S.; Gallo L. C. Discovery of the Narrow-Line Seyfert 1 Galaxy Markarian 335 in a Historical Low X-Ray Flux State. *ApJ* 2007, 668, L111
41. Grupe D. et al. XMM-Newton Observations of the Narrow-Line Seyfert 1 Galaxy Mrk 335 in a Historical Low X-Ray Flux State. *ApJ* 2008, 681, 982
42. Gallo L. C. et al. A blurred reflection interpretation for the intermediate flux state in Mrk 335. *MNRAS* 2013, 428, 1191
43. Kara E.; Fabian A. C.; Cackett E. M.; Uttley P.; Wilkins D. R.; Zoghbi A. Discovery of high-frequency iron K lags in Ark 564 and Mrk 335. *MNRAS* 2013, 434, 1129
44. Wilkins D. R.; Gallo L. C. Driving extreme variability: the evolving corona and evidence for jet launching in Markarian 335. *MNRAS* 2015, 449, 129
45. Wilkins D. R.; Gallo L. C.; Grupe D.; Bonson K.; Komossa S.; Fabian, A. C. Flaring from the supermassive black hole in Mrk 335 studied with Swift and NuSTAR. *MNRAS* 2015, 454, 4440
46. Gallo L. C.; Blue D. M.; Grupe D.; Komossa S.; Wilkins D. R. Eleven years of monitoring the Seyfert 1 Mrk 335 with Swift: Characterizing the X-ray and UV/optical variability. *MNRAS* 2018, 478, 2557
47. Gallo L. C. et al. Evidence for an emerging disc wind and collimated outflow during an X-ray flare in the narrow-line Seyfert 1 galaxy Mrk 335. *MNRAS* 2019, 484, 4287

48. Wilms J.; Allen A.; McCray R. On the Absorption of X-Rays in the Interstellar Medium. *ApJ* 2000, 542, 914
49. Arnaud K. A. XSPEC: The First Ten Years. *A.S.P. Conference Series*, 1996, 101, 17
50. Kalberla P. M. W.; Burton W. B.; Hartmann D.; Arnal E. M.; Bajaja E.; Morras R.; Poppel W. G. L. The Leiden/Argentine/Bonn (LAB) Survey of Galactic HI. Final data release of the combined LDS and IAR surveys with improved stray-radiation corrections. *A&A* 2005, 440, 775
51. Magdziarz P.; Zdziarski A. A. Angle-dependent Compton reflection of X-rays and gamma-rays. *MNRAS* 1995, 273, 837
52. Mondal S.; Chakrabarti S. K.; Nagarkoti, S.; Arevalo, P. Possible range of viscosity parameter to trigger black hole candidates to exhibit different states of outbursts. *ApJ* 2017, 850, 47
53. Mastroserio G.; Ingram A.; van der Klis M. Multi-timescale reverberation mapping of Mrk 335. *MNRAS* 2020, 498, 4971
54. Garcia et al. X-Ray Reflection Spectroscopy of the Black Hole GX 339–4: Exploring the Hard State with Unprecedented Sensitivity. *ApJ* 2015, 813, 84
55. Chainakun P.; Young A. J. Simultaneous spectral and reverberation modelling of relativistic reflection in Mrk 335. *MNRAS* 2015, 452, 333
56. Ezhikode, S. H.; Dewangan, G. C.; Misra, R.; Philip, N. S. Correlation between relativistic reflection fraction and photon index in NuSTAR sample of Seyfert 1 AGN. *MNRAS*, 2020, 495, 3373
57. Reeves et al. On why the Iron K-shell absorption in AGN is not a signature of the local Warm/Hot Intergalactic Medium. 2008, *MNRAS*, 385L, 108
58. Chakrabarti S. K. Estimation and effects of the mass outflow from shock compressed flow around compact objects. *A&A* 1999, 351, 185
59. Chakrabarti S. K. Spectral signature of mass loss (and mass gain by) an accretion disk around a black hole. *ApJ* 2002, 579L, 21
60. Mondal S.; Chakrabarti S. K.; Debnath D. Spectral signatures of dissipative standing shocks and mass outflow in presence of Comptonization around a black hole. *Ap&SS* 2014, 353, 223
61. Chatterjee D.; Debnath D.; Jana A.; Chakrabarti S. K. Properties of the black hole candidate XTE J1118+480 with the TCAF solution during its jet activity induced 2000 outburst. *Ap&SS* 2019, 364, 14
62. Chakrabarti S. K. & Wiita, P. J. Spiral Shocks in Accretion Disks As a Contributor to Variability in Active Galactic Nuclei. *ApJ* 1993, 411, 602
63. Komossa S. et al. Lifting the curtain: The Seyfert galaxy Mrk 335 emerges from deep low-state in a sequence of rapid flare events. *A&A* 2020, 643L, 7
64. Parker M. L. et al. The nuclear environment of the NLS1 Mrk 335: Obscuration of the X-ray line emission by a variable outflow. *MNRAS* 2019, 490, 683
65. Sarma R.; Tripathi S.; Misra R.; Dewangan G.; Pathak A.; Sarma J. K. Relationship between X-ray spectral index and X-ray Eddington ratio for Mrk 335 and Ark 564. *MNRAS* 2015, 448, 1541

Appendix A

Here we show the spectral fitting plots for the rest of the observations using all three models.

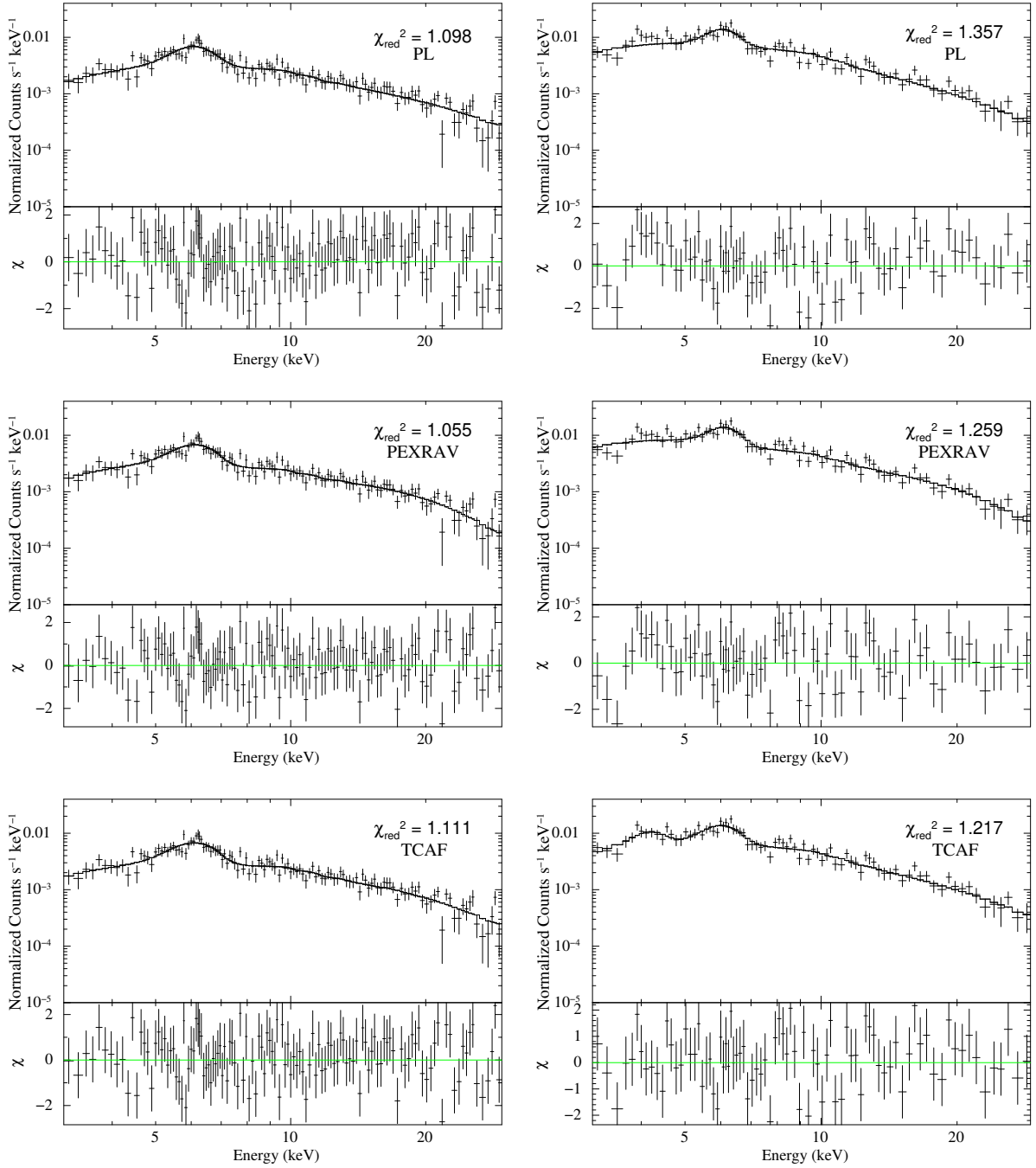


Figure A1. Same as Figure 2 but for the OBSIDs 80201001002 (left panel) and 90602619004 (right panel) along with the residuals.

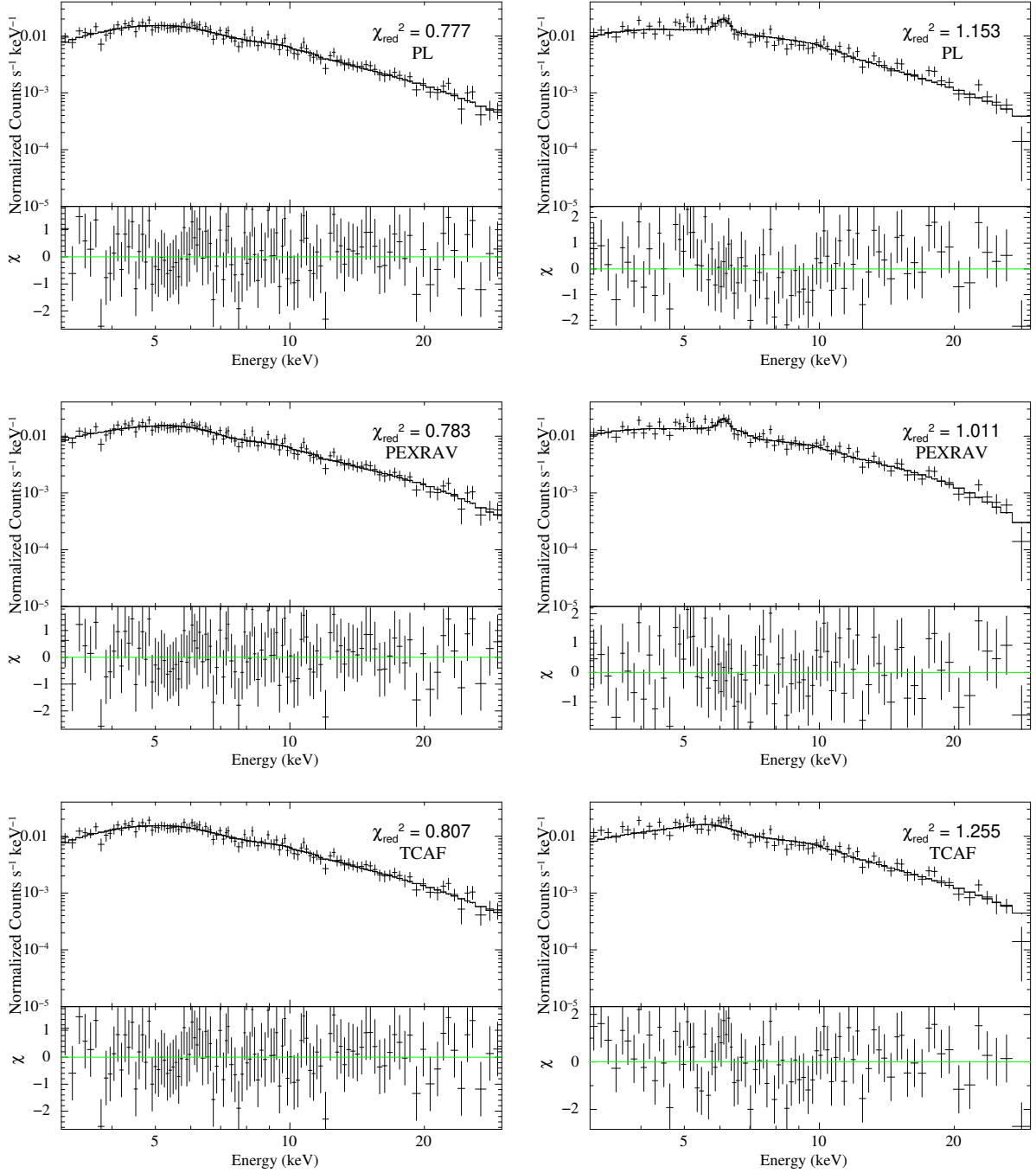


Figure A2. Same as Figure 2 but for the OBSIDs 90602619006 (left panel) and 90602619008 (right panel) along with the residuals.